

The Strong Field QED approach of the vacuum interaction processes at ELI-NP

M. Pentia,^{1,*} C.R. Badita,¹ D. Dumitriu,¹ A.R. Ionescu,¹ and H. Petrascu¹

¹*IFIN-HH, National Institute for Physics and Nuclear Engineering,
Reactorului 30, RO-077125, POB-MG6 Bucharest-Magurele, Romania*

(Dated: September 1, 2023)

The commissioning of the high power laser facility Extreme Light Infrastructure - Nuclear Physics (ELI-NP) at Bucharest-Măgurele (Romania) allows the in-depth study of nonlinear interactions in Strong Field Quantum Electrodynamics (SF-QED). The present paper analyzes the SF-QED processes possible to study at ELI-NP. Carrying out such experiments will allow finding answers to many fundamental QED questions. Firstly it needs to highlight and evaluate the various interactions with the virtual particles of the QED vacuum as the processes of multi-photon inverse Compton scattering, e^+e^- pair production, e^+e^- pair annihilation, e^-e^- Moller scattering, e^+e^- Bhabha scattering, electron self-energy, photon self-energy or vacuum energy. In this sense, the current worldwide results are analyzed along with the main steps necessary for the design of SF-QED experiments at ELI-NP.

After a brief review of the first experiment (E-144 SLAC) which confirmed the existence of nonlinear QED interactions of high-energy electrons with photons of a laser beam, we presented the fundamental QED processes that can be studied at ELI-NP in the multi-photon regime along with the characteristic parameters of the laser beam used in the QED interaction with electrons.

To prepare an experiment at ELI-NP, it is necessary to analyze both the kinematics and the dynamics of the interactions. Therefore, we first reviewed the kinematics of linear QED processes and then the corresponding Feynman diagrams. For nonlinear, non-perturbative multi-photon QED interactions, the Feynman diagram technique must be adapted from linear to nonlinear processes. This is done by switching to quantum fields described by Dirac-Volkov dressed states of particles in an intense electromagnetic (EM) field. This allows the evaluation of the amplitude of the physical processes and finally the determination of the cross-sections of these processes.

SF-QED processes of multi-photon interactions with strong laser fields can be investigated taking into account the characteristics of the ELI-NP facility in the context of QED vacuum pair production of electron-positron pairs and energetic gamma rays.

Finally, we present some similar experimental projects from other research centers, in different stages of implementation.

I. INTRODUCTION

In 2009 G.V. Dunne (University of Connecticut) [1] remarked "the ELI project opens up an entirely new non-perturbative regime of QED and of quantum field theories in general. There are many experimental and theoretical challenges ahead. Theoretically, the biggest challenge in the non-perturbative arena is to develop efficient techniques, both analytical and numerical, for computing the effective action and related quantities, in external fields that realistically represent the experimental laser configurations. A lot of progress has been made in this direction, but new ideas and methods are still needed".

Most of the high power laser works interpret the SF-QED interactions as non-perturbative processes, relative to the classical field-matter interaction strength ξ and quantum parameter χ (see later). For experimental studies must be evaluated the cross sections of these processes. Therefore, the treatment of SF-QED processes must be done in terms of vacuum interaction processes with Feynman diagrams for "dressed" particle in oscillatory EM fields [2]. The treatment of non-perturbative QED has a different meaning than that of

non-perturbative QCD. The last one is connected with the strong coupling parameter α_s , which is too large for a perturbative approach. On the other hand, the non-perturbative QED regime is characterized by the coupling parameter ξ between the matter and the laser field. Here we are dealing with SF-QED interactions but we do not appeal to the QED coupling constant $\alpha \approx 1/137$ as parameter of perturbative developments, but to the coupling ξ between matter and the laser field, which can exceed the unit. As such, processes and diagrams of given order in α (Feynman diagrams) depend on all terms of the expansion in ξ . On the other hand, the electron-laser interactions are described by particle "dressed" states [3] as it comes to have multi-photon interactions, and by high-order processes with radiative corrections in the theory.

Today, the ELI-NP facility can provide laser beams of 2×10 PW with intensities up to $10^{22} - 10^{23} \text{ W/cm}^2$ [4–6]. Therefore, we can proceed to initiate experimental works for the in-depth study of nonlinear QED processes. With such laser beams can be performed a series of works as:

- Systematic studies of the dynamics of fundamental QED processes possible to approach at high power lasers and to evaluate the amplitude of these processes such as: γe inverse Compton scattering [7–11], Breit-Wheeler e^+e^- pair production [12], Bethe-Heitler e^+e^- pair production [13], Dirac

* Corresponding author: pentia@nipne.ro

e^+e^- pair annihilation, e^-e^- Moller Scattering, e^+e^- Bhabha Scattering, Electron Self Energy, Photon Self Energy, Vacuum Energy [14].

- Proposal of experimental works for the measurement of physical properties related to the production of e^+e^- pairs (Schwinger mechanism) in the photon-multi-photon interaction (Breit-Wheeler nonlinear), the multi-photon-virtual photon interaction of the nucleus field (Bethe-Heitler nonlinear), or the production and measurement of QED (positronium) bound states.
- Design and carry out experimental works to measure some fundamental processes using high-power lasers at ELI-NP.

The production of a large number of positrons with MeV energies opens the door to new avenues of anti-matter research, including understanding the physics of various processes and phenomena in astrophysics, such as black holes and gamma-ray bursts [15, 16], or from pair plasma physics [17, 18].

II. FUNDAMENTAL GAMMA-ELECTRON INTERACTIONS

The conversion of laser light to matter is one of the fundamental processes of EM photon-photon interaction, less experimentally studied so far. This is one of the spectacular predictions of QED, but difficult to achieve. The reason is due both to a reduced photon-photon cross section (~ 0.1 barn), but mainly due to the difficulty of achieving an adequate density of photon beams [12].

However, E.J. Williams [19] noted that sufficiently high photon densities can be obtained in the intense electric field of a nucleus in relativistic motion. Therefore, the production of pairs of particles from the EM field is possible to achieve in principle:

- In a static electric field - the Schwinger effect [20];
- In a photonic field - Breit-Wheeler production [12, 21, 22];
- In a combination of the two - Bethe-Heitler production [13].

Such linear QED laser light - matter interaction processes are shown in Fig.1 in the form of Feynman diagrams. They can be studied at the ELI-NP facility, but in the laser multi-photon oscillatory EM field, as nonlinear interactions of "dressed" particles [2].

Current theoretical and experimental works with high-power lasers (see for example [23]) have highlighted the possibility of experimental study of some fundamental QED interactions such as:

- Linear Breit-Wheeler interaction process (Fig.2.a): $\gamma + \gamma \rightarrow e^+ + e^-$ with electron-positron pair production, treated in linear QED [24].

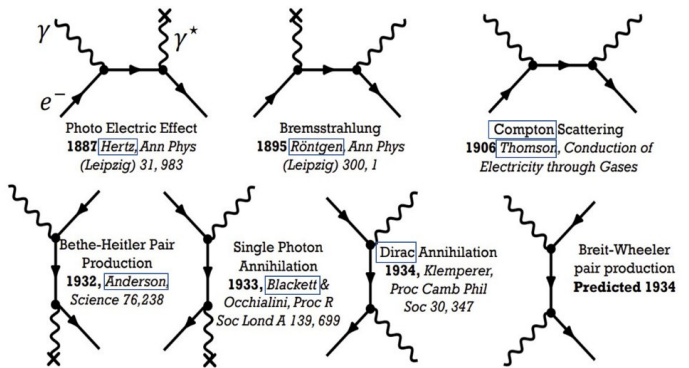


FIG. 1. Light (γ) and matter (e^-) QED interaction processes. (thanks to Oliver Pick presentation 23 October 2014, LNFN – Frascati, "Observing the two-photon Breit-Wheeler process for the first time", underlined - Nobel laureates)

- Nonlinear inverse Compton scattering (multi-photon) (Fig.2.b): $e^- + n\gamma_L \rightarrow e^- + \gamma$, where the initial electron interacts with n laser photons γ_L and is emitted a γ photon of high energy. Up to 40% of the energy of the initial electrons is transferred to the final photon [25].
- Nonlinear (multi-photon) Breit-Wheeler interaction process (Fig.2.c): $\gamma + n\gamma_L \rightarrow e^+ + e^-$, pair production, with the energy of several laser photons transformed into the mass of electron-positron pairs [26].
- The Bethe-Heitler interaction process with the intense electric field of the nucleus (Fig.2.d): $n\gamma_L + \gamma_V \rightarrow e^+ + e^-$, where the $n\gamma_L$ the laser multi-photon interaction with γ_V virtual photon of the intense field of the nucleus, leads to e^+e^- pair production [13].

A. QED vacuum interaction processes

Under normal conditions, the physical vacuum, due to quantum fluctuations, is in a permanent state of "boiling", with the creation and annihilation of virtual particle-antiparticle pairs. According to the Heisenberg principle, locally, on short time intervals Δt , there are energy fluctuations ΔE , so that their product is not smaller than \hbar : $\Delta E \cdot \Delta t \geq \hbar$. On time intervals Δt , the ΔE fluctuation can produce e^+e^- pairs, at shallow depth under the mass shell. That is, $\Delta E \approx 2m_e c^2 = 2 \cdot 0.511 \text{ MeV} \approx 10^6 \text{ eV}$ and $\Delta t \geq \hbar / 2m_e c^2 = 10^{-22} \text{ s}$. So, locally, the process of e^+e^- pair production is confined in a spatial interval Δx and temporal Δt , after which the pair annihilates (see Fig.3.a)). This process of production and annihilation of virtual e^+e^- pairs is associated with the vacuum polarization phenomenon.

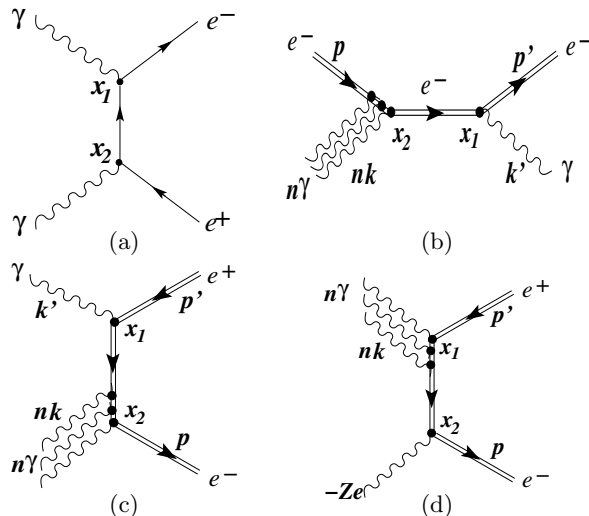


FIG. 2. a) Breit-Wheeler linear process; b) Nonlinear inverse Compton scattering (multi-photon); c) Nonlinear Breit-Wheeler process (multi-photon); d) Nonlinear Bethe-Heitler interaction.

If an external electric field E transfers enough energy to these virtual pairs during Δt (see Fig.3.b)) it can transform them into real pairs that can be observed and recorded experimentally.

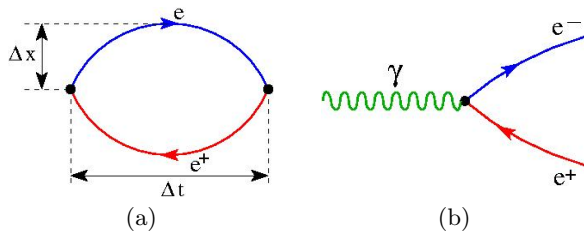


FIG. 3. a) Vacuum fluctuations with creation and annihilation of virtual e^+e^- pairs; b) Energy transfer from the EM field ensures the virtual pairs separation and their transformation into real pairs.

The characteristic distance $2\Delta x$ over which the electric field can produce real e^+e^- pairs is given by the reduced Compton wavelength λ_c ,

$$2\Delta x \approx 2c\Delta t = \frac{\hbar}{m_e c} = \lambda_c \approx 386 \cdot 10^{-15} \text{ m} \quad (1)$$

The real e^+e^- pair will be produced if a minimum energy W is transferred from the field E ,

$$W = e E \lambda_c = \frac{e E \hbar}{m_e c} > 2m_e c^2 \quad (2)$$

Hence the minimum value of the electric field leading to vacuum breakdown is:

$$E > \frac{2m_e^2 c^3}{\hbar e} = 2E_{cr} \quad (3)$$

In the case of a uniform EM field, this defines the Schwinger limit of the critical electric field E_{cr} capable of producing vacuum breakdown, i.e. the starting value of the spontaneous real e^+e^- pairs production in the laser field - vacuum interaction:

$$E_{cr} = \frac{m_e^2 c^3}{\hbar e} = 1.323 \cdot 10^{18} \text{ V/m} \quad (4)$$

Other words, the value (4) specifies the minimum electric field capable of performing on an electron the work $\epsilon_e = W/2$ over the Compton wavelength λ_c , equal to its rest mass $m_e c^2$:

$$\epsilon_e = e E_{cr} \lambda_c = m_e c^2 \quad (5)$$

The value (4) of the Schwinger critical electric field E_{cr} has not yet been reached experimentally. This field leading to vacuum breakdown with the production of e^+e^- pairs (Breit-Wheeler process), presents a lot of nonlinear aspects.

The field intensities accessible in the laboratory system nowadays are three orders of magnitude lower than the value of the critical field E_{cr} . However, in the rest system of a high energy electron, it "sees" the transverse component of the laser electric field E boosted by γ_e (Lorentz factor) and reaches a value $E^* = \gamma_e E$.

Based on the relationship between the electric field E and the intensity of the laser beam I_L : $E(\text{V/m}) = 2750\sqrt{I_L} (\text{W/cm}^2)$, for the ELI-NP with the intensity $I_L > 10^{22} \text{ W/cm}^2$, light pulses lead to field intensity $E \approx 10^{14} \text{ V/m}$ at the focal point, on a distance of several laser wavelengths. For example, with an electron beam energy of $\epsilon_e = 10 \text{ GeV}$, the Lorenz factor is $\gamma_e = \epsilon_e/m_e c^2 \approx 2 \cdot 10^4$ so that if a laser beam collides head-on, it "sees" a boosted laser field $E^* \approx 2 \cdot 10^{18} \text{ V/m}$. Therefore, the intensity of the laser field in the moving electron system will be of the order of critical value E_{cr} (4).

B. First matter-light conversion experiment (E-144 SLAC)

In the SLAC E-144 experiment [25–28], studies of nonlinear QED processes were carried out using 46.6 GeV electrons scattered on the intense laser EM field with a wavelength of 527 nm (2.35 eV), see Fig.4. Using peak focused laser in pulses of the order of terawatt and energy of 650 mJ, intensities of 10^{18} W/cm^2 were obtained.

The production of e^+e^- pairs requires an energy in the center of mass system at least of $2m_e c^2 = 1.02 \text{ MeV}$. This can be achieved by a nonlinear Breit-Wheeler process, i.e. by scattering on a laser beam a high-energy photon created by inverse Compton scattering of a laser beam on a high-energy electron (see Fig.4).

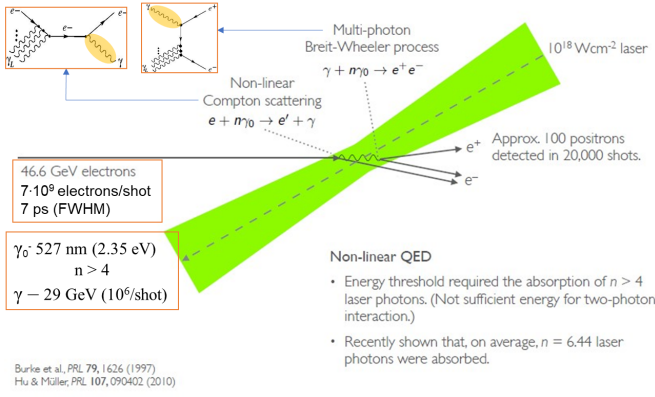


FIG. 4. The SLAC E-144 experiment. Positron production process in $\gamma\gamma$ scattering (O.Pike, <https://agenda.infn.it/event/8532/contributions/74190>)

For the production of pairs from the interaction $\gamma_1\gamma_2 \rightarrow e^+e^-$, having laser light γ_1 of wavelength 527 nm (energy 2.35 eV), would require photons γ_2 of energy 109 GeV. But with 527 nm laser photons scattered on a 46.6 GeV electron beam available at SLAC, the maximum energy of the nonlinear Compton scattered photons is only 29.2 GeV [28]. Therefore it is necessary to use both the relativistic electron boost and a multi-photon interaction process. The electric field increase is obtained by the relativistic boost of the counter-propagating electron with the energy in the laboratory system ϵ_e by a Lorentz factor $\gamma_e = \epsilon_e/m_e c^2 \gg 1$. Then the electron "sees" the E_L laser field boosted to the value $E^* = \gamma_e E_L$. So, for $\epsilon_e = 46.6$ GeV, the electron with Lorentz factor $\gamma_e = 46.6 \cdot 10^3 \text{ MeV}/0.511 \text{ MeV} = 9 \cdot 10^4$ colliding head-on with a 527 nm laser photon, "sees" the field in its rest frame $E^* = 1.1 \cdot 10^{18} \text{ V/m}$. This is close to the Schwinger limit $E_{cr} = m_e^2 c^3/\hbar e = 1.3 \cdot 10^{18} \text{ V/m}$, which can transfer to an electron, along a Compton wavelength, the energy equal to its rest mass, at which a static electric field would vacuum spontaneously break-down into e^+e^- pairs.

To reach the value of the critical field E_{cr} , we must resort to multi-photon and electron interactions with a high-intensity laser I_L , which in this way ensures a sufficiently strong electric field E_L , according to $I_L = \epsilon_0 c \langle E_L^2 \rangle$ (see later) (24).

The parameters of the experiment correspond to the nonlinear Compton regime (see Fig.5). The high-energy photon resulting from inverse Compton scattering interacts with the multi-photon laser beam and produces e^+e^- pairs through the nonlinear Breit-Wheeler process (see Fig.6).

Important Note: Linear, single-photon QED interaction processes described by Feynman diagrams such as those in Fig.1, can be studied in the multi-photon regime using the same Feynman diagrams, but with "dressed" (Dirac-Volkov) particle states and propagators [2] because the particle is moving in the oscillating EM field.

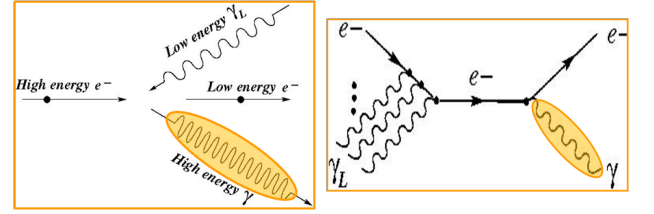


FIG. 5. High-energy photon production by inverse Compton scattering of laser beams. a) Kinematics of the Compton inverse scattering; b) Feynman diagram for determining the amplitude.

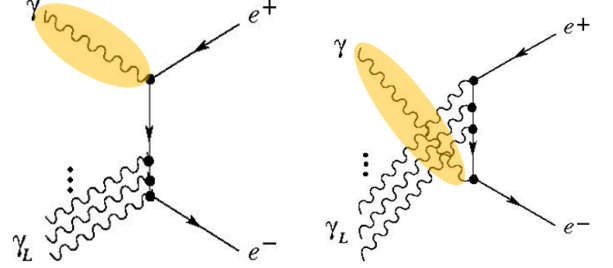


FIG. 6. Feynman diagrams for the production of e^+e^- pairs by the nonlinear Breit-Wheeler process.

III. GAMMA - ELECTRON SCATTERING

A. Kinematics of the $e_i \gamma_i \rightarrow e_f \gamma_f$ scattering

The 4-momentum conservation, see Fig.7:

$$q_{\gamma i} + q_{e i} = q_{\gamma f} + q_{e f} \quad (6)$$

By squaring (6), with $q_{\gamma}^2 = 0$ and $q_e^2 = m_e^2 c^2$, we have:

$$q_{\gamma i} \cdot q_{e i} = q_{\gamma f} \cdot q_{e f} \quad (7)$$

Multiply (6) by $q_{\gamma f}$ and using (7) we have:

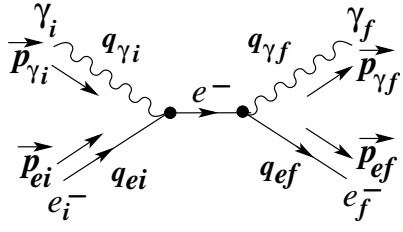
$$q_{\gamma f} \cdot (q_{\gamma i} + q_{e i}) = q_{\gamma i} \cdot q_{e i} \quad (8)$$

Expressing (8) by 3-components, with the notations of Fig.8, we get the energy $\epsilon_{\gamma f}$ of the final photon as a function of the energy $\epsilon_{\gamma i}$ of the initial photon for a given electron energy $\epsilon_{e i}$:

$$\epsilon_{\gamma f} = \frac{\epsilon_{\gamma i} \epsilon_{e i} (1 - \beta_{e i} \cos \alpha_i)}{\epsilon_{\gamma i} (1 - \cos \theta) + \epsilon_{e i} (1 - \beta_{e i} \cos \alpha_f)} \quad (9)$$

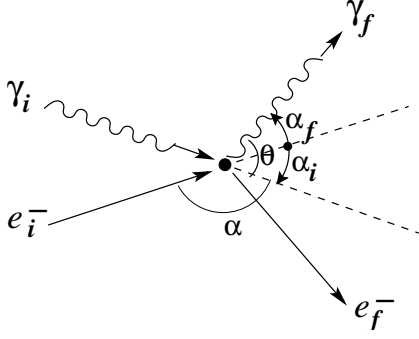
In the initial electron rest frame: $\beta_{e i} = 0$; $\gamma_{e i} = 1$; $\epsilon_{e i} = m_e c^2$ the photon energy change is:

$$\frac{\epsilon_{\gamma f}}{\epsilon_{\gamma i}} = \frac{1}{1 + \frac{\epsilon_{\gamma i}}{m_e c^2} (1 - \cos \theta)} \quad (10)$$



$$\begin{aligned} \epsilon_\gamma &= h\nu & \vec{p}_\gamma &= \frac{\epsilon_\gamma}{c} \vec{n}_\gamma \\ \epsilon_e &= \gamma_e m_e c^2 & \vec{p}_e &= \gamma_e m_e \vec{v}_e = \frac{\epsilon_e}{c^2} \vec{v}_e = \frac{\epsilon_e}{c} \vec{\beta}_e \\ q &\equiv \left(\frac{E}{c}, \vec{p} \right) & \text{metric: } & g_{\mu\mu} = (1, -1, -1, -1) \\ q^2 &= \frac{E^2}{c^2} - \vec{p}^2 = m_e^2 c^2 \end{aligned}$$

$q_{\gamma i} = \frac{\epsilon_{\gamma i}}{c} (1, \vec{n}_{\gamma i})$	$q_{\gamma f} = \frac{\epsilon_{\gamma f}}{c} (1, \vec{n}_{\gamma f})$	$\beta_e = \frac{p_e c}{\epsilon_e} = \frac{v_e}{c}$
$q_{e i} = \frac{\epsilon_{e i}}{c} (1, \vec{\beta}_{e i})$	$q_{e f} = \frac{\epsilon_{e f}}{c} (1, \vec{\beta}_{e f})$	$\gamma_e = \frac{\epsilon_e}{m_e c^2} = \frac{1}{\sqrt{1 - \beta_e^2}}$

FIG. 7. $e_i \gamma_i \rightarrow e_f \gamma_f$ scattering variables and kinematicsFIG. 8. Kinematics of the $\gamma_i e_i^- \rightarrow \gamma_f e_f^-$ scattering

Multiply (8) by q_{ei} , we have:

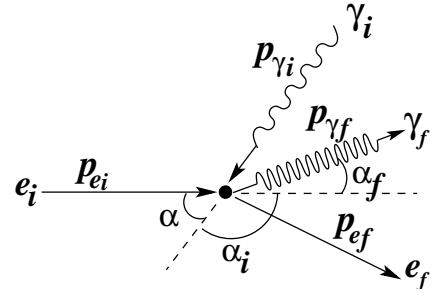
$$q_{\gamma f} = \frac{(q_{\gamma i} \cdot q_{ei}) q_{ei}}{(q_{\gamma i} \cdot q_{ei}) + m_e^2 c^2} \quad (11)$$

The temporal component gives the energy dependence of the final photon on the initial electron energy:

$$\epsilon_{\gamma f} = \frac{(q_{\gamma i} \cdot q_{ei}) \epsilon_{ei}}{(q_{\gamma i} \cdot q_{ei}) + m_e^2 c^2} \quad (12)$$

where (see Fig.9)

$$q_{\gamma i} \cdot q_{ei} = \frac{\epsilon_{\gamma i} \epsilon_{ei}}{c^2} (1 + \beta_{ei} \cos \alpha) \quad (13)$$

FIG. 9. The high energy γ_f -ray production geometry by inverse Compton scattering

That is, the final photon energy (12) is

$$\epsilon_{\gamma f} = \frac{\epsilon_{ei}}{1 + \frac{m_e^2 c^4}{\epsilon_{\gamma i} \epsilon_{ei}} (1 + \beta_{ei} \cos \alpha)} \quad (14)$$

B. The dressed electron mass in the electromagnetic field

The motion of a free electron in an EM field can be described in terms of the interaction of the electron with a classical plane wave of frequency ω . In general, such an electron will show an oscillatory motion with the same frequency ω and will radiate in turn. For a circularly polarized laser, EM waves with electric and magnetic components E_L and B_L have a constant amplitude and rotate with the angular frequency ω_L in a plane perpendicular to the direction of wave propagation. In this wave, the movement of the electron is circular with radius r , angular frequency ω_L and tangential speed $v_\perp = \omega_L r$ perpendicular to the direction of movement, parallel to the magnetic field vector B_L [29].

The circular motion of the electron is $m_e v_\perp^2 / r = e E_L$ or

$$p_\perp \omega_L = e E_L \quad (15)$$

where $p_\perp = \gamma m_e v_\perp$ is the electron transverse momentum.

For a relativistic electron we have $\beta_\perp = p_\perp c / \epsilon_e$ and $\gamma = \epsilon_e / m_e c^2$ and the transverse momentum will be:

$$p_\perp = \beta_\perp \gamma m_e c \quad (16)$$

The product:

$$\xi = \beta_\perp \gamma \quad (17)$$

defines the *field strength parameter*.

A relativistic electron inside an EM plane wave field appears to have an "increased" mass. Indeed, based on the energy - mass relation of the electron:

$$\begin{aligned} m_e^2 c^2 &= \frac{\epsilon_e^2}{c^2} - \vec{p}^2 & \text{with (16) and (17)} \\ m_e^2 c^2 &= \frac{\epsilon_e^2}{c^2} - p_\parallel^2 - \xi^2 m_e^2 c^2 \end{aligned} \quad (18)$$

the relativistic energy of the electron in an EM field, now is:

$$\frac{\epsilon_e^2}{c^2} - p_{\parallel}^2 = m_e^2 c^2 (1 + \xi^2) \quad (19)$$

where p_{\parallel} is the longitudinal momentum parallel to the direction of propagation of the wave. Heuristically, one can say that the electron behaves as if it had an effective mass [7]:

$$\bar{m}_e = m_e \sqrt{1 + \xi^2} \quad (20)$$

This behavior is identifiable by a shift in the kinematic edge for Compton scattering, such that, the electron in an EM plane wave field is moving along the p_{\parallel} and behaves as having a "dressed" mass \bar{m}_e .

Although this mass "increase" has been derived classically, the same relation (20) for the effective mass appears in the quantum treatment of the solutions of the Dirac equation for free electrons in the EM plane wave as Dirac-Volkov "dressed" states [2].

C. Classical laser intensity parameter ξ (nonlinearity charge-field coupling)

The electric field strength parameter ξ (17) can be expressed with the transverse momentum (16) or in connection (15) with the electric field component E_L or, as we will see, with the intensity I_L of the laser beam. For the moment it can be write:

$$\xi = \beta_{\perp} \gamma = \frac{e E_L}{m_e \omega_L c} \quad (21)$$

The Lorentz factor $\gamma = 1/\sqrt{1 - \beta_{\perp}^2}$ with (17) can be expressed as: $\gamma = 1/\sqrt{1 + \xi^2}$ and $\beta_{\perp} = \xi/\sqrt{1 + \xi^2}$.

Then the radius of electron's circular trajectory is less than the reduced laser wavelength $\lambda_L = \lambda_L/(2\pi)$:

$$r = \frac{v_{\perp}}{\omega_L} = \frac{\beta_{\perp} c}{\omega_L} = \frac{\xi}{\sqrt{1 + \xi^2}} \frac{\lambda_L}{2\pi} \leq \frac{\lambda_L}{2\pi} \quad (22)$$

Now, it is convenient to redefine the parameter ξ by squaring (21) as:

$$\xi^2 = \frac{e^2 \langle E_L^2 \rangle}{m_e^2 \omega_L^2 c^2} \quad (23)$$

where the average $\langle E_L^2 \rangle$ is taken with respect to time.

The ξ^2 (23) measures the average laser beam intensity I_L expressed as usual in electro-dynamics by $\langle E_L^2 \rangle$:

$$I_L = \epsilon_0 c \langle E_L^2 \rangle \quad (24)$$

With the mean laser electric field as the r.m.s.

$$E_L \approx \sqrt{\langle E_L^2 \rangle} = \sqrt{\frac{1}{\epsilon_0 c}} \sqrt{I_L} \quad \text{or} \quad E_L = 1944 \cdot \sqrt{I_L} \quad \text{for} \quad I_L \text{ in } W/cm^2 \quad (25)$$

Substituting $\langle E_L^2 \rangle$ from (25) in (23) with $\omega_L = 2\pi c/\lambda_L$, we get finally:

$$\xi^2 = 3.65 \times 10^{-19} I_L \lambda_L^2 \quad \text{for } I_L \text{ in } W/cm^2 \text{ and } \lambda_L \text{ in } \mu m \quad (26)$$

At ELI-NP for a laser wavelength $\lambda_L = 0.815 \mu m$ and the pulse intensity at the focus $I_L \sim 10^{22} W/cm^2$, we have $\xi \cong 50$.

D. Physical interpretation of the laser intensity parameter ξ

The laser intensity is connected with the energy transfer from the laser field to electron [30]. The classical laser intensity parameter ξ (21) can be interpreted with the work of the laser field over the electron Compton wavelength λ_c :

$$\xi = \frac{e E_L}{m_e c \omega_L} = e E_L \frac{\lambda_c}{\hbar \omega_L} = e E_L \frac{\lambda_L}{m_e c^2} \quad (27)$$

$$\text{where} \quad \lambda_c = \frac{\hbar}{m_e c} \quad ; \quad \lambda_L = \frac{c}{\omega_L}$$

The product $e E_L \lambda_c$ represents the work of the laser field E_L over the electron reduced Compton wavelength λ_c (see Fig.10). ξ (27) is measuring this work in units of photon energy $\hbar \omega_L$. So ξ gives the number of laser photons interacting along the λ_c .

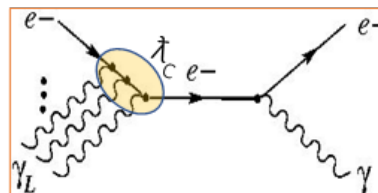


FIG. 10. Electron multi-photon laser interaction.

ξ is a classical parameter, because it is independent of \hbar and it measures the laser intensity as the number n of γ_L laser photons interacting with the electron along the Compton wavelength λ_c .

Also, the last term of Eq. (27) can be interpreted as the energy transfer to the electron over the laser wavelength λ_L in units of electron rest mass $m_e c^2$.

If we consider the Schwinger electric field threshold E_{cr} (4), the ξ parameter can be expressed as:

$$\xi = \frac{m_e c^2}{\hbar \omega_L} \frac{E_L}{E_{cr}} = \frac{\lambda_L}{\lambda_c} \frac{E_L}{E_{cr}} \quad (28)$$

The smallness of the factor E_L/E_{cr} is compensated by the large ratio of laser to Compton wavelength λ_L/λ_c of the order 10^6 [30].

The ξ parameter value encodes certain processes as:

- $\xi \ll 1$: the processes with minimum possible number of photons are the most probable. The probabilities equal the perturbation (linear) theory probabilities and plane waves play the role of individual photons.
- $\xi \sim 1$ or $\xi > 1$: the probabilities to absorb different number of photons become comparable and the process becomes multi-photon, i.e., the probability has an essentially non-perturbative (nonlinear) dependence on the field.
- $\xi \gg 1$: the case of modern laser technology.

E. Quantum nonlinearity parameter χ_e

As long as ξ parameter (27) is given in relation to the photon field energy transfer over a reduced Compton wavelength $e E_L \lambda_c$ (in $\hbar\omega_L$ units), the quantum χ_e parameter is defined in terms of the energy of the electron ϵ_e (in $m_e c^2$ units) and the laser field E_L (in E_{cr} units):

$$\chi_e = \frac{\epsilon_e}{m_e c^2} \frac{E_L}{E_{cr}} = \gamma_e \frac{E_L}{E_{cr}} = \gamma_e \frac{\hbar\omega_L}{m_e c^2} \xi \quad (29)$$

here we used (28) to express connection with ξ .

If laser field is $E_L = E_{cr}$ and electron energy (5) $\epsilon_e = \epsilon_{cr} = e E_{cr} \lambda_c = m_e c^2$ is the work performed by the field E_L over reduced Compton wavelength λ_c , then $\chi_e = 1$. This way χ_e compares the $\gamma_e E_L$ field strength in the rest frame of the electron, with the critical field E_{cr} and measures the importance of quantum nonlinear effects in e^+e^- vacuum pair production [8, 31].

In the context of SF-QED, the quantum nonlinearity parameter χ_e serves as a measure of the importance of nonlinear QED processes such as multi-photon Compton scattering, e^+e^- pair production and photon-photon scattering. These processes become significant when the quantum nonlinearity parameter is of order unity or greater.

IV. LINEAR QED INTERACTION PROCESSES

The Feynman diagrams allows to determine the invariant amplitude of the QED processes, the \hat{S} matrix elements and finally the cross section for the studied process. The Feynman diagrams of the interested linear QED processes are shown in Table I.

Evaluation of the Feynman diagrams uses the electromagnetic $\hat{A}_\mu(x)$ and Dirac $\hat{\psi}(x)$ and $\hat{\bar{\psi}}(x)$ field operators with the corresponding annihilation and creation compo-

nents listed below:

$$\left\{ \begin{array}{l} \hat{A}_\mu(x) = \int \frac{d^3\vec{k}}{(2\pi)^3} \frac{1}{2\omega} \left[\underbrace{\hat{a}_\lambda(\vec{k}) \epsilon_\mu^\lambda e^{-i\vec{k}\cdot x}}_{\sim \hat{A}_\mu^-(x)} + \underbrace{\hat{a}_\lambda^\dagger(\vec{k}) \epsilon_\mu^\lambda e^{i\vec{k}\cdot x}}_{\sim \hat{A}_\mu^+(x)} \right] \\ \hat{\psi}(x) = \sum_s \int \frac{d^3\vec{p}}{(2\pi)^3} \frac{m}{\omega} \left[\underbrace{\hat{b}_s(\vec{p}) u_s(\vec{p}) e^{-i\vec{p}\cdot x}}_{\sim \hat{\psi}^-(x)} + \underbrace{\hat{c}_s^\dagger(\vec{p}) v_s(\vec{p}) e^{i\vec{p}\cdot x}}_{\sim \hat{\psi}^+(x)} \right] \\ \hat{\bar{\psi}}(x) = \sum_s \int \frac{d^3\vec{p}}{(2\pi)^3} \frac{m}{\omega} \left[\underbrace{\hat{c}_s(\vec{p}) \bar{v}_s(\vec{p}) e^{-i\vec{p}\cdot x}}_{\sim \hat{\bar{\psi}}^-(x)} + \underbrace{\hat{b}_s^\dagger(\vec{p}) \bar{u}_s(\vec{p}) e^{i\vec{p}\cdot x}}_{\sim \hat{\bar{\psi}}^+(x)} \right] \end{array} \right.$$

where the field operators act with corresponding annihilation and creation operators:

$$\begin{array}{l} \hat{A}_\mu^-(x) \rightarrow \hat{a} - \text{photon annihilation in } x \\ \hat{\psi}^-(x) \rightarrow \hat{b} - \text{electron annihilation in } x \\ \hat{\bar{\psi}}^-(x) \rightarrow \hat{c} - \text{positron annihilation in } x \\ \hline \hat{A}_\mu^+(x) \rightarrow \hat{a}^\dagger - \text{photon creation in } x \\ \hat{\psi}^+(x) \rightarrow \hat{c}^\dagger - \text{positron creation in } x \\ \hat{\bar{\psi}}^+(x) \rightarrow \hat{b}^\dagger - \text{electron creation in } x \end{array} \quad (30)$$

An example, for evaluation of the Feynman diagrams Fig.11 of the Compton (photon-electron) scattering, imply determination of the \hat{S} matrix elements: $\langle \gamma, e^- | \hat{S}_A | \gamma, e^- \rangle$ and $\langle \gamma, e^- | \hat{S}_B | \gamma, e^- \rangle$.

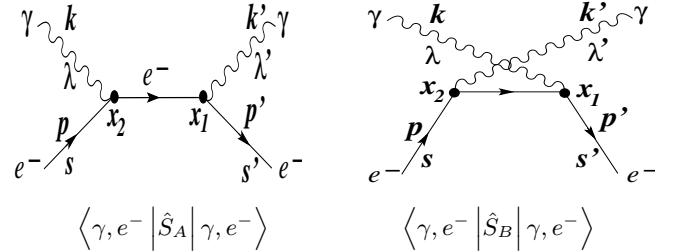


FIG. 11. Feynman diagrams for the photon - electron (Compton) scattering

Using the appropriate creation/annihilation components, the scattering matrix for the two diagrams in Fig.11, are:

$$\begin{array}{l} \text{crea.} \quad \text{crea.} \quad \text{an.} \quad \text{an.} \\ e^- \quad \gamma \quad \gamma \quad e^- \\ \downarrow \quad \downarrow \quad \downarrow \quad \downarrow \\ \hat{S}_A = - \left(\frac{e}{\hbar} \right)^2 \int d^4x_1 d^4x_2 N \left(\hat{\bar{\psi}}^+ \hat{A}^+ \hat{\psi}^- \right)_{x_1} \left(\hat{\bar{\psi}}^+ \hat{A}^- \hat{\psi}^- \right)_{x_2} \\ \\ \text{crea.} \quad \text{an.} \quad \text{crea.} \quad \text{an.} \\ e^- \quad \gamma \quad \gamma \quad e^- \\ \downarrow \quad \downarrow \quad \downarrow \quad \downarrow \\ \hat{S}_B = - \left(\frac{e}{\hbar} \right)^2 \int d^4x_1 d^4x_2 N \left(\hat{\bar{\psi}}^+ \hat{A}^- \hat{\psi}^- \right)_{x_1} \left(\hat{\bar{\psi}}^+ \hat{A}^+ \hat{\psi}^- \right)_{x_2} \end{array}$$

The above contractions are expressed by corresponding S_F Feynman propagators between $x_2 \rightarrow x_1$ (see Fig.11).

TABLE I. The Feynman diagrams of some linear QED processes and the corresponding \hat{S} matrix elements

Process	Feynman diagrams	\hat{S} matrix element
photon-electron scattering $\gamma + e^- \rightarrow \gamma + e^-$ photon-positron scattering $\gamma + e^+ \rightarrow \gamma + e^+$		$\langle \gamma, e^- \hat{S} \gamma, e^- \rangle$ $\langle \gamma, e^+ \hat{S} \gamma, e^+ \rangle$
$e^+ e^-$ pair annihilation $e^- + e^+ \rightarrow \gamma + \gamma$		$\langle \gamma, \gamma \hat{S} e^-, e^+ \rangle$
$e^+ e^-$ pair production $\gamma + \gamma \rightarrow e^- + e^+$		$\langle e^-, e^+ \hat{S} \gamma, \gamma \rangle$
e^- Møller scattering $e^- + e^- \rightarrow e^- + e^-$ e^+ Møller scattering $e^+ + e^+ \rightarrow e^+ + e^+$		$\langle e^-, e^- \hat{S} e^-, e^- \rangle$ $\langle e^+, e^+ \hat{S} e^+, e^+ \rangle$
$e^- + e^+$ Bhabha scattering $e^- + e^+ \rightarrow e^- + e^+$		$\langle e^-, e^+ \hat{S} e^-, e^+ \rangle$
Electron self energy $e^- \rightarrow e^-$ Positron self energy $e^+ \rightarrow e^+$		$\langle e^- \hat{S} e^- \rangle$ $\langle e^+ \hat{S} e^+ \rangle$
Photon self energy $\gamma \rightarrow \gamma$		$\langle \gamma \hat{S} \gamma \rangle$
Vacuum energy Vacuum \rightarrow Vacuum		$\langle 0 \hat{S} 0 \rangle$

$$\overbrace{\hat{\psi}^-(x_1)\hat{\psi}^+(x_2)} = iS_F(p+k)$$

$$\overbrace{\hat{\psi}^-(x_1)\hat{\psi}^+(x_2)} = iS_F(p-k')$$

Individual invariant amplitude \mathcal{M}_i is evaluated for each Feynman diagram relative to \hat{S}_i matrix element. The \hat{S} matrix element is given by total amplitude \mathcal{M}_{fi} and the phase space volume of the process:

$$\langle \gamma, e^- | \hat{S} | \gamma, e^- \rangle = (2\pi)^4 \delta^4(p+k-p'-k') \mathcal{M}_{fi} \quad (31)$$

where the total amplitude \mathcal{M}_{fi} is the sum of individual amplitudes:

$$\begin{cases} \mathcal{M}_{fi} = \mathcal{M}_{fi}^A + \mathcal{M}_{fi}^B \\ \mathcal{M}_{fi}^A = -\left(\frac{e}{\hbar}\right)^2 \bar{u}_{s'}(\vec{p}') \not{\epsilon}_{\lambda'} iS_F(p+k) \not{\epsilon}_{\lambda} u_s(\vec{p}) \\ \mathcal{M}_{fi}^B = -\left(\frac{e}{\hbar}\right)^2 \bar{u}_{s'}(\vec{p}') \not{\epsilon}_{\lambda'} iS_F(p-k') \not{\epsilon}_{\lambda} u_s(\vec{p}) \end{cases} \quad (32)$$

This allows the determination of the cross section for $\gamma + e \rightarrow \gamma + e'$ scattering.

Similarly, the cross sections for the other QED processes from Table I could be evaluated.

V. SF-QED INTERACTION PROCESSES

The SF-QED process can be understood as an interaction of an electron with a plane wave EM field of frequency ω . In general, such an electron will exhibit oscillatory motion and in turn will radiate. Therefore, to calculate the \hat{S} matrix elements of the SF-QED processes, the technique of Feynman diagrams can be used, with the field states and propagators this time as dressed Dirac-Volkov state operators, with particles of effective mass \bar{m}_e (20) and effective 4-momentum q_μ inside the field [2]:

$$q_\mu = p_\mu + \frac{\xi^2 m^2}{1(k \cdot p)} k_\mu \quad (33)$$

where k_μ is the wave (laser) photon 4-momentum.

The Feynman rules summarized in [29], but used now for SF-QED processes, with our notations (30), are:

1. External incoming or outgoing electrons are represented by laser dressed Volkov state operator $\hat{\psi}^-(x)$ (annihilation) or $\hat{\psi}^+(x)$ (creation), respectively. For incoming and outgoing positrons, one uses the corresponding Volkov state operators $\hat{\psi}^-(x)$ (annihilation) and $\hat{\psi}^+(x)$ (creation).
2. An internal fermion line corresponds to the Dirac-Volkov propagator $\mathcal{G}(x, y)$.
3. Internal and external photon lines are translated into the free photon propagator and the free photon states, respectively, see e.g. [14].

4. Each interaction vertex corresponds to a factor $-ie\gamma^\mu$ and an integral d^4x .
5. Symmetry factors for identical particles are the same as in usual QED.

A. The nonlinear inverse Compton scattering

The first interaction process of the free electrons with strong EM fields we consider the nonlinear Compton scattering [2, 7–9, 11, 33] in which an electron absorbs multiple photons and radiates a single high-energy photon (see Fig.12):

$$e + n\gamma_L \rightarrow e' + \gamma \quad (34)$$

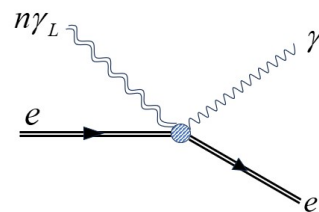


FIG. 12. The nonlinear Compton scattering. A dressed electron e^- in a strong EM field (double line) absorbs n photons γ_L (double sinusoids) and emits a high-energy photon γ and recoils as e' .

To study the SF-QED processes it is necessary to draw the corresponding Feynman diagrams with dressed particles to evaluate the invariant amplitude and finally to obtain the cross section.

In the experimental works with high power lasers, the inverse Compton scattering processes are used as the sources of the high energy photons (see Fig.5).

B. Bremsstrahlung

Another process as a source of high energy gammas is bremsstrahlung interaction (see Fig.13).

As an example, the ultra-relativistic electrons lose energy in a gold target almost solely by bremsstrahlung. The produced gamma rays in a particular arrangement [10] have the distributions presented in Fig.14.

C. Breit-Wheeler pair production

The high-energy gamma photons obtained from the previous processes of inverse Compton scattering or bremsstrahlung can interact with a multi-photon laser beam and as these photons propagate through the laser field can interact to produce electron-positron pairs:

$$\gamma + n\gamma_L \rightarrow e^+ + e^- \quad (35)$$

This is referred to as multi-photon Breit-Wheeler pair production and can be regarded as the materialization of

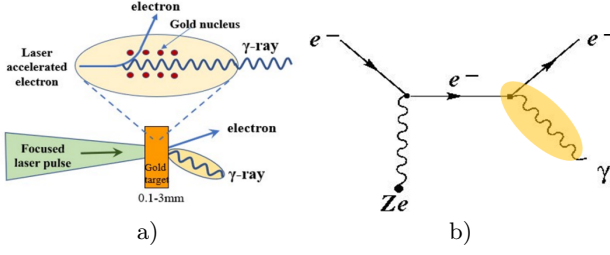


FIG. 13. a) Experimental arrangement of the bremsstrahlung process; b) Feynman diagram of bremsstrahlung (the double line dressed electrons are not drawn).

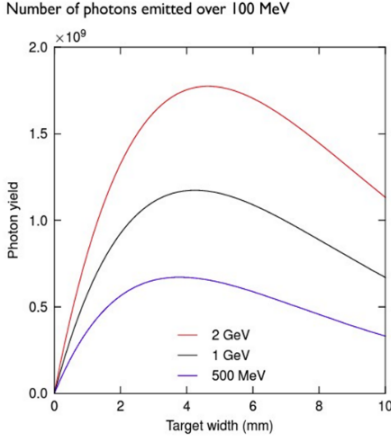


FIG. 14. High-energy photon distribution emitted from the gold target [10]

a vacuum-polarization loop in a strong field. The cross section of the nonlinear Breit-Wheeler pair creation can be evaluated with the Feynman type diagrams Fig.15, with dressed electrons (not drawn with double line in the figure).

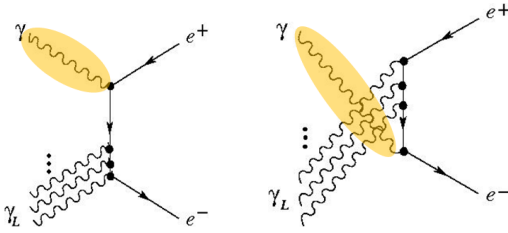


FIG. 15. Feynman diagrams for $\gamma + n\gamma_L \rightarrow e^+ + e^-$ Breit-Wheeler e^+e^- pair production (the double line dressed electrons are not drawn).

D. Bethe-Heitler pair production

A process of e^+e^- pair production possible to be studied at ELI-NP is the interaction of the previously obtained high energy photons (by inverse Compton scatter-

ing or bremsstrahlung) with virtual photons of a strong EM field of the atomic nucleus.

$$\gamma + \gamma_V \rightarrow e^+ + e^- \quad (36)$$

The evaluation of the cross section is done with the Feynman type diagrams Fig.16, but with the dressed electrons.

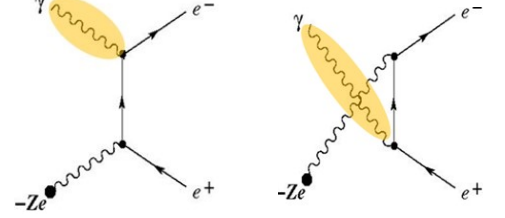


FIG. 16. Feynman diagrams for Bethe-Heitler process (the double line dressed electrons are not drawn).

Another possible Bethe-Heitler e^+e^- pairs production is by multi-photon laser interaction with the virtual photons of an atomic nucleus field:

$$n\gamma + \gamma_V \rightarrow e^+ + e^- \quad (37)$$

The evaluation of the cross section of this e^+e^- pairs production in the field of the atomic nucleus is done with the Feynman type diagrams in Fig.17.

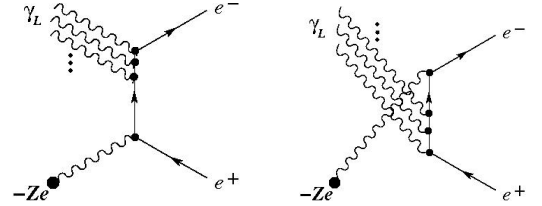


FIG. 17. Feynman diagrams for multi-photon Bethe-Heitler e^+e^- pair production (the double line dressed electrons are not drawn).

VI. ELI-NP EXPERIMENTAL FACILITY

The facilities at ELI-NP allow for the first time the use of the two 10 PW laser beams with intensities up to $10^{22} - 10^{23} \text{ W/cm}^2$ to study strong-field nonlinear QED interaction processes with laser beams [4, 32]. The two 10 PW laser beams are extracted from the same laser pulse by splitting it into two pulses and are amplified on two identical amplifier chains. The two 10 PW pulses must be coherent. However, variations in the optical path traveled by the two pulses require additional adjustments to be made for "femtosecond" level synchronization.

There are two main types of experiments that could be performed (see Fig.18).

In the first experiment Fig.18.a), using one of the 10 PW laser beams as the pump-laser focused with a large

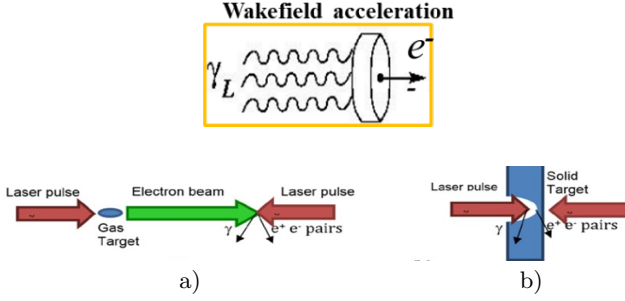


FIG. 18. The two 10 PW laser pulses (red arrows) for SF-QED studies with gas (a) and solid (b) targets (I.C.E. Turcu et al. [32])

focal length mirror (F/20) on a gaseous target (gas jet or gas cell) which produces, by wakefield acceleration, relativistic electrons ($\gamma_e \gg 1$), see Fig.19. The second high-intensity 10 PW probe-laser beam is focused with an F/3 mirror onto the relativistic electron bunch, Fig.19. Being exposed to the strongly focused laser field, they generate intense gamma rays and electron-positron pairs, through the nonlinear QED interaction processes that we intend to study.

The laser intensity of 10 PW focused in the focal spot with a diameter of $5 \mu\text{m}$ is expected to be greater than 10^{22} W/cm^2 . The pump and probe-laser are synchronized and delayed relative to each other as required. High-energy gamma photons can be measured with a gamma detector placed before the electron beam-dump. On the other hand, electron and positron spectra can be measured with dedicated spectrometers Fig.19.

In the second experiment Fig.18.b), the 10 PW pump-laser is tightly focused by an F/3 mirror on a foil-solid target and produces relativistic electrons. The second laser, the 10 PW probe-laser is also tightly focused by an F/3 mirror on a solid target and then conveniently delayed relative to the pump-laser. The probe-laser produces a strong EM field to which the electrons are exposed. The solid target method is complementary to the gas target method. In the latter case, the number of relativistic electrons is very high, the target being a solid. This number is much higher than in the gas target or beam-beam method. On the other hand, the kinetic energy of the electrons is no longer as high as in the "beam-beam" method.

ELI-NP can prepare the E6 experimental area and the interaction chamber with the gas target, shown in Fig.19. The chamber contains the two pump & probe colliding 10 PW laser beams. Measuring the characteristics of interacting SF-QED processes in intense laser fields is an experimental challenge: it requires high-sensitivity detectors for electrons and positrons in the presence of very high background levels of X-radiation and γ photons.

The experimental area E6 with the two counter-propagating 10 PW laser beams focused on the gas and the solid target, can be prepared at ELI-NP. The required equipment and configuration of the E6 experimen-

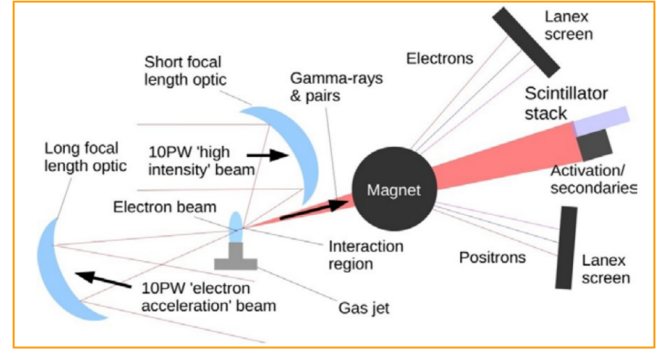


FIG. 19. Layout of the gas target experimental components for the study of SF-QED processes (Reprinted from [32])

TABLE II. E6 experimental chamber (laser-gas interaction)

<p><u>E6 equipment consists of:</u></p> <ul style="list-style-type: none"> • 24 m^3 interaction chamber • ISO-7 clean room • Opto-mechanical components • Gas targets of various types • 30 m long focal, large aperture spherical mirror • Laser and Plasma Diagnostics (1st or 2nd harmonic) • Multi GeV electron spectrometers • Gamma ray spectrometer
<p><u>E6 target area configuration (gas targets, QED)</u></p> <ul style="list-style-type: none"> • 2 \times 10 PW laser beams: 240 J, 23 fs, 810 nm, ~ 45 cm dia. FWHM • or 10 PW @ 1/60 Hz and 1 PW @ 1 Hz • 1 Short focal - parabolic mirrors F2.7 • 1 Long focal ~ 30 m - spherical mirror \sim F60 @ 10 PW (\sim F160 @ 1 PW) • 1 Plasma mirror • 1 Cleanroom • Experimental chamber: $L \times W \times H$ of $4000 \times 3300 \times 1780 \text{ mm}^3$

tal chamber with gas target are presented in Table II.

The possibilities presented by Keita Seto et al. [34] are shown in the diagram for the physical regime offered by ELI-NP (see Fig.20). The high intensity of the ELI-NP laser allows obtaining a number of photons participating in an interaction $N > 10^5$ (see the star in Fig.20). The use of photons from 10 keV up to the GeV class should be considered.

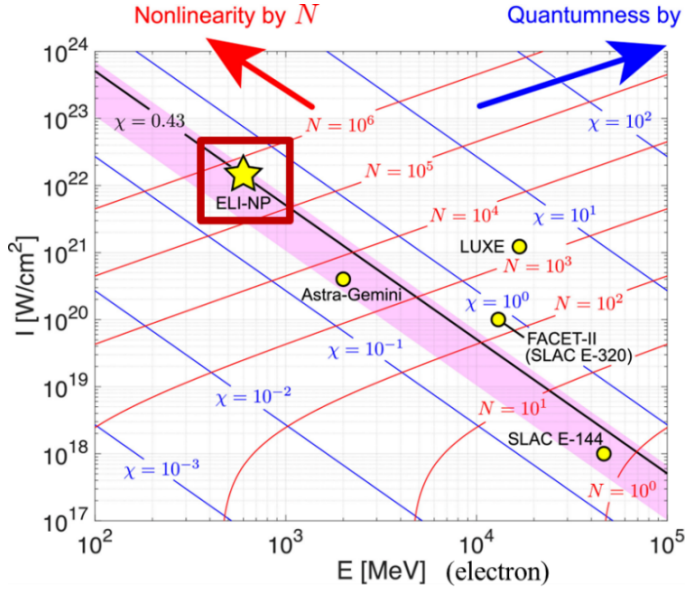


FIG. 20. The curves at given N and χ . N is the number of absorbed laser photon and χ is intensity parameter. The pink ribbon represents the domain as $\chi \in [0.2, 0.5]$. We consider "linear" Compton scattering in the area where $N \leq 1$ (a single laser photon absorption). The star symbol shows the parameter set at ELI-NP [34].

VII. UCOMING EXPERIMENTS

Several petawatt-class lasers have been built worldwide. Currently, multi-PW and even 10 PW lasers have been built or are being planned to be built around the world [35]. Some of them have proposals to study fundamental processes in SF-QED regime in order to explore non-perturbative effects. These upcoming experiments include:

- **LUXE (Laser Und XFEL Experiment)** is a new experiment proposed at DESY and the European XFEL to study QED in the strong-field regime where QED becomes non-perturbative. It aims at studying high-field QED in electron-laser and photon-laser interactions, with the 16.5 GeV electron beam of the XFEL and a laser beam with power of up to 350 TW. The experiment will measure the spectra of electrons, positrons and photons [36].

- **ASTRA-GEMINI** (Central Laser Facility, STFC Rutherford Appleton Laboratory, Harwell Oxford, Dicot, UK) [11].

- **E-320 experiment at FACET-II**, SLAC will collide 13 GeV electrons with 10 TW laser pulses, to study fundamental strong-field QED processes [37].

- **Apollon** in France. The ultra-intense and highly focused Apollo pulses make it possible to study the ultra-relativistic laser-plasma interaction regime, nonlin-

ear Compton/Thomson scattering from laser-accelerated electron beams, the production of pairs in the presence of strong Coulombian fields [38].

Other laser facilities with active SF-QED study programs include:

- **ZEUS facility at the University of Michigan**, once commissioned (late 2023), will use two laser pulses (with 2.5 PW and 0.5 PW), one to accelerate electrons in a laser wakefield accelerator (to either 10 GeV, or several GeV) and one to provide the EM field (with intensity 10^{21} W/cm², or 10^{23} W/cm²), will allow exploration of fundamental yet unanswered questions regarding nonlinear quantum electrodynamics in relativistic plasmas, including quantum radiation reaction and electron-positron pair production mechanisms [39].

- **SEL Station of Extreme Light (SEL)** facility in China, will be completed in 2025 and then open to users a 100-PW laser facility. It can provide focused intensity of more than 10^{23} W/cm² [40].

- **ELI-BL in Czech Republic**

<https://www.eli-beams.eu/>

- **CALA in Germany**

<http://cala-laser.de/experiments/hf.html>

- **J-Karen in Japan**,

<https://doi.org/10.3390/qubs1010007>

- **CORELS in Korea**

https://corels.ibs.re.kr/html/corels_en/

VIII. CONCLUSIONS

Here we presented the theoretical framework for the main SF-QED vacuum interaction processes possible to be studied at ELI-NP and the experimental possibilities offered by this laser infrastructure. The kinematics and dynamics of these processes were presented for evaluation of the amplitudes necessary for cross section determination.

We analyzed the early experimental results as well as the new approaches of similar projects around the world. Based on these results, we can move on to the preparation, design and implementation of the experimental works to test some fundamental SF-QED interactions. For this purpose, it is necessary to go through some essential stages of the experimental studies at ELI-NP.

It will be necessary to:

- evaluate the cross sections for the processes proposed to be studied
- simulate the physical interaction processes
- preparation of the characteristic distributions on the available phase-space for these processes

- detector system design to cover the available phase-space
- the evaluation of the required statistics of the experimental data to achieve significant results to verify the QED predictions.
- implementation of the detector system and performance of the experimental works.

Based on the results of this work, it is possible to proceed to the next stage of the design and realization of the experimental studies of the SF-QED processes at ELI-NP.

The proposed experimental configuration include:

- gas targets with the pump-laser beam focused by a long focal length (F/20 or F/80) mirror to drive a wakefield for electron bunch acceleration to multi-

GeV energies and then exposed to the EM field of the probe-laser tightly focused (F/3).

- solid targets with the pump and probe-laser beams focused on the target.
- vacuum QED experiments without any target but with similar interaction geometries and diagnostics to the ones above.

ACKNOWLEDGMENTS

This work was supported by Institute of Atomic Physics and the Ministry of Research, Innovation and Digitalization under program ELI-NP-RO, Contract 8/ELI-RO (2020) - Romania.

-
- [1] G.V. Dunne, New strong-field QED effects at extreme light infrastructure, *Eur. Phys. J. D* 55, 327-340 (2009).
- [2] D. M. Volkov, Uber eine Klasse von Losungen der Diracschen Gleichung, *Z. Phys.* 94, 250 (1935).
- [3] V. I. Ritus, Quantum effects of the interaction of elementary particles with an intense electromagnetic field, *J. Sov. Laser Res.* 6(5), 497-617 (1985).
- [4] I. C. E. Turcu et al., Quantum electrodynamics experiments with colliding petawatt laser pulses, *High Power Laser Sci. Eng.* 7, e10 (2019).
- [5] F. Negoita et al., Laser driven nuclear physics at ELI-NP, *Rom. Rep. Phys.* 68, S37-S144 (2016)
- [6] S. Gales et al., The extreme light infrastructure-nuclear physics (ELI-NP) facility: new horizons in physics with 10 PW ultra-intense lasers and 20 MeV brilliant gamma beams, *Rep. Prog. Phys.* 81(9), 094301 (2018).
- [7] T. W. B. Kibble, Frequency shift in high-intensity Compton scattering, *Phys. Rev.* 138(3B), B740 (1965).
T. W. B. Kibble, Mutual refraction of electrons and photons, *Phys. Rev.* 150(4), 1060 (1966).
T. W. B. Kibble, Refraction of electron beams by intense electromagnetic waves, *Phys. Rev. Lett.* 16(23), 1054 (1966).
T. W. Kibble, *Cargese Lectures in Physics*, vol. M. Levy. (1968).
- [8] V. B. Berestetskii, E. M. Lifshitz & L. P. Pitaevskii, *Quantum Electrodynamics: Volume 4*, Butterworth-Heinemann (1982).
- [9] H. Chen et al., Relativistic Positron Creation Using Ultraintense Short Pulse Lasers, *Phys. Rev. Lett.* 102(10), 105001 (2009)
- [10] O. Pike et al., A photon-photon collider in a vacuum hohlraum, *Nature Photonics* 8, 434 (2014)
- [11] S. Rose, Using thermal radiation fields to investigate QED processes with high-power lasers, Seminar held at Imperial College London, <https://lasers.llnl.gov/content/assets/docs/nif-workshops/user-group-2020/Steven-Rose.pdf>
- [12] G. Breit & J. A. Wheeler, Collision of two light quanta, *Phys. Rev.* 46(12), 1087 (1934).
- [13] H. Bethe & W. Heitler, On the stopping of fast particles and on the creation of positive electrons, *Proc. R. Soc. Lond. Ser. A-Contain. Pap. Math. Phys. Character* 146(856), 83-112 (1934).
- [14] M. E. Peskin & D. V. Schroeder, *An introduction to quantum field theory*, Addison-Wesley Publishing Company (1995).
- [15] J. F. C. Wardle et al., Electron-positron jets associated with the quasar 3C279, *Nature*, 395(6701), 457-461 (1998).
- [16] P. Meszaros, Theories of gamma-ray bursts, *Annu. Rev. Astron. Astrophys.* 40(1), 137-169 (2002).
- [17] H. A. Weldon, Measuring T_c of the quark-gluon plasma with e^+e^- pairs, *Phys. Rev. Lett.* 66(3), 293 (1991).
- [18] E. G. Blackman & G. B. Field, Ohm's law for a relativistic pair plasma, *Phys. Rev. Lett.* 71(21), 3481 (1993).
- [19] E. J. Williams, Nature of the High Energy Particles of Penetrating Radiation and Status of Ionization and Radiation Formulae, *Phys. Rev.* 45, 729 (1934)
- [20] F. Sauter, On the behavior of an electron in a homogeneous electric field in Dirac's relativistic theory, *Zeit. f. Phys.* 69(742), 45 (1931)
W. Heisenberg & H. Euler, Folgerungen aus der diracschen theorie des positrons, *Zeit. F. Phys.*, 98(11-12), 714-732 (1936)
J. Schwinger, On gauge invariance and vacuum polarization, *Phys. Rev.* 82(5), 664 (1951).
- [21] H. R. Reiss, Absorption of light by light, *J. Math. Phys.* 3(1), 59-67 (1962).
- [22] N. B. Narozhny et al., Quantum Processes in the Field of a Circularly Polarized Electromagnetic Wave, *Sov. Phys. JETP* 20, 622 (1965).
- [23] A. Fedotov, A. Ilderton, F. Karbstein, B. King, D. Seipt, H. Taya, G. Torgrimsson, Advances in QED with intense background fields, *Phys. Rep.* 1010, 1-138 (2023).
- [24] W. Greiner & J. Reinhardt, *Quantum electrodynamics*, Springer Science & Business Media (2008).
- [25] C. Bula, et al., Observation of nonlinear effects in Compton scattering, *Phys. Rev. Lett.* 76(17), 3116 (1996).
- [26] E-144 Collaboration, C. Bamber et al., Positron produc-

- tion in multi-photon light-by-light scattering, AIP Conf. Proc. 396(1), 165-177, (1997).
- [27] D. L. Burke et al., Positron production in multiphoton light-by-light scattering, Phys. Rev. Lett. 79(9), 1626 (1997).
- [28] C. Bamber et al., Studies of nonlinear QED in collisions of 46.6 GeV electrons with intense laser pulses, Phys. Rev. D 60(9), 092004 (1999).
- [29] D. Seipt, Volkov states and nonlinear Compton scattering in short and intense laser pulses, arXiv preprint arXiv:1701.03692 (2017).
- [30] T. Heinzl, A. Ilderton, A Lorentz and gauge invariant measure of laser intensity, Optics Comm. 282, 1879 (2009).
- [31] T. G. Blackburn et al., Benchmarking semiclassical approaches to strong-field QED: Nonlinear Compton scattering in intense laser pulses, Phys. Plasmas 25, 083108 (2018).
- [32] I.C.E. Turcu et al., High field physics and QED experiments at ELI-NP, Rom. Rep. Phys 68, S145 (2016).
I.C.E. Turcu, S Balascuta, F.Negoita, D.Jaroszynski, P.McKenna, Strong field physics and QED experiments with ELI-NP 2x10PW laser beams, AIP Conference Proceedings 1645, 416 (2015)
- [33] O. Pike et al., Observing the two-photon Breit-Wheeler process for the first time, APS-DPP Meeting Abstracts 2014, UO7-007 (2014).
- [34] K. Seto, J.F. Ong, Y. Nakamiya, M. Cuciuc, M.M. Rosu, V.R M. Rodrigues, O. Tesileanu, K.A. Tanaka, Experimental design of radiation reaction by 1 PW laser pulse and linear accelerator electron bunch, High Energy Density Physics 38, 100919 (2021)
- [35] C. N. Danson et al., Petawatt and exawatt class lasers worldwide, High Power Laser Sci. Eng. 7, e54 (2019).
- [36] H. Abramowicz et al., Letter of intent for the LUXE experiment, arXiv preprint arXiv:1909.00860 (2019)
H. Abramowicz et al., Conceptual design report for the LUXE experiment, Eur. Phys. J. Spec. Top. 230(11), 2445-2560 (2021)
M. Wing and the LUXE collaboration, Detector challenges of the strong-field QED experiment LUXE at the European XFEL, Seminar held at CERN, (2023).
- [37] S. Meuren, Probing strong-field QED at FACET-II (SLAC e-320), Third conference on extremely high intensity laser physics, 7 (2019)
S. Meuren, E-320: Probing Strong-field QED at FACET-II, FACET-II PAC Meeting (2020)
F. C. Salgado et al., Single particle detection system for strong-field QED experiments, New J. Phys. 24(1), 015002 (2021).
- [38] D. N. Papadopoulos et al., The Apollon 10 PW laser: experimental and theoretical investigation of the temporal characteristics, High Power Laser Sci. Eng. 4, e34 (2016).
- [39] S. Cole Johnson, The ZEUS laser is the most powerful laser in the U.S.-featuring chirped-pulse amplification and a multi-laser beam capability, Laser Focus World (2022).
- [40] X. Wang et al., 13.4 fs, 0.1 Hz OPCPA front end for the 100 PW-class laser facility, Ultrafast Science (2022).